Proteome-wide cellular thermal shift assay reveals unexpected cross-talk between brassinosteroid and auxin signaling

Qing Lu[a,b], Yonghong Zhang[a,b,1], Joakim Hellner[c], Caterina Giannini[d], Xiangyu Xu[a,b], Jarne Pauwels[e,f], Qian Ma[a,b], Wim Dejonghe[a,b], Huibin Han[d,2], Brigitte Van de Cotte[a,b], Francis Impens[e,f,g], Kris Gevaert[e,f], Ive De Smet[a,b], Jiří Friml[d], Daniel Martinez Molina[c], and Eugenia Russinova[a,b,3]

[a]Department of Plant Biotechnology and Bioinformatics, Ghent University, 9052 Ghent, Belgium; [b]Center for Plant Systems Biology, VIB, 9052 Ghent, Belgium; [c]Pelago Bioscience AB, 171 48 Solna, Sweden; [d]Institute of Science and Technology Austria, 3400 Klosterneuburg, Austria; [e]Department of Biomolecular Medicine, Ghent University, 9052 Ghent, Belgium; [f]Center for Medical Biotechnology, VIB, 9052 Ghent, Belgium; and [g]VIB Proteomics Core, 9052 Ghent, Belgium

Edited by Natasha Raikhel, Center for Plant Cell Biology, Riverside, CA; received October 4, 2021; accepted January 31, 2022

Despite the growing interest in using chemical genetics in plant research, small molecule target identification remains a major challenge. The cellular thermal shift assay coupled with high-resolution mass spectrometry (CETSA MS) that monitors changes in the thermal stability of proteins caused by their interactions with small molecules, other proteins, or posttranslational modifications, allows the discovery of drug targets or the study of protein–metabolite and protein–protein interactions mainly in mammalian cells. To showcase the applicability of this method in plants, we applied CETSA MS to intact *Arabidopsis thaliana* cells and identified the thermal proteome of the plant-specific glycogen synthase kinase 3 (GSK3) inhibitor, bikinin. A comparison between the thermal and the phosphoproteomes of bikinin revealed the auxin efflux carrier PIN-FORMED1 (PIN1) as a substrate of the *Arabidopsis* GSK3s that negatively regulate the brassinosteroid signaling. We established that PIN1 phosphorylation by the GSK3s is essential for maintaining its intracellular polarity that is required for auxin-mediated regulation of vascular patterning in the leaf, thus revealing cross-talk between brassinosteroid and auxin signaling.

cellular thermal shift assay | chemical genetics | brassinosteroids | auxin

Although the application of chemical genetics to plant research is gaining interest (1–3), unraveling the mode of action of the small molecules remains a major challenge. The cellular thermal shift assay (CETSA) is a label-free method that can assess target engagement directly in live cells (4), but its application to plant cells remains limited (5, 6). The technique is based on the biophysical principle that a ligand can induce changes in the thermal stability of the target protein, allowing the generation of so-called protein melting curves (7, 8). Similar to the classical thermal shift assay with purified proteins, small molecule binding typically leads to protein stabilization and an increase in melting temperature (T_m). Coupling CETSA with multiplexed quantitative mass spectrometry (MS) enables the monitoring of an entire proteome for changes in protein thermostability in the presence of a small molecule (9, 10). Consequently, proteins interacting with this molecule can be identified without previous knowledge of the pathways or molecular mechanisms involved (11). As the thermal stability of a protein may also be affected by posttranslational modifications or by binding to other proteins, cofactors, or metabolites, CETSA MS carried out on intact cells, in which active signaling takes place, allows the identification of effector proteins downstream of the direct target (9).

The small molecule bikinin (12) is an inhibitor specifically targeting the *Arabidopsis thaliana* Shaggy/glycogen synthase kinase 3 (GSK3)-like kinases (*At*SKs), including the key negative brassinosteroid (BR) signaling regulator BR-INSENSITIVE2 (BIN2)/*At*SK21 that phosphorylates and inactivates two main transcription factors, BRASSINAZOLE RESISTANT1 (BZR1) and BRI1-EMS-SUPPRESSOR1 (BES1)/BZR2 (13, 14). The *Arabidopsis* genome encodes 10 *At*SKs, which belong to four groups (15); evidence exists for at least six, *At*SK11, *At*SK12, *At*SK13, *At*SK22, *At*SK23, and *At*SK32, that negatively regulate the BR signaling just as BIN2/*At*SK21 (16–18). Like the mammalian GSK3s (19), *At*SKs also phosphorylate numerous substrates and control many developmental and physiological processes in plants, such as root, stomatal, and flower development; xylem differentiation; responses to light; and different abiotic and biotic stresses (15). BIN2/*At*SK21 also mediates the cross-talk between BR and other plant hormones, including auxin (15).

Despite the reported interdependency and cooperation (20–25), the molecular mechanisms of the signaling cross-talk between BRs and auxin are still not well understood. Although auxin does not affect the phosphorylation state of the BZR1

Significance

Chemical genetics, which investigates biological processes using small molecules, is gaining interest in plant research. However, a major challenge is to uncover the mode of action of the small molecules. Here, we applied the cellular thermal shift assay coupled with mass spectrometry (CETSA MS) to intact *Arabidopsis* cells and showed that bikinin, the plant-specific glycogen synthase kinase 3 (GSK3) inhibitor, changed the thermal stability of some of its direct targets and putative GSK3-interacting proteins. In combination with phosphoproteomics, we also revealed that GSK3s phosphorylated the auxin carrier PIN-FORMED1 and regulated its polarity that is required for the vascular patterning in the leaf.

Author contributions: Q.L., J.F., and E.R. designed research; Q.L., Y.Z., J.H., C.G., X.X., J.P., Q.M., W.D., H.H., B.V.d.C., F.I., K.G., I.D.S., and D.M.M. performed research; Q.L., J.H., C.G., X.X., J.P., H.H., F.I., K.G., I.D.S., J.F., D.M.M., and E.R. analyzed data; and Q.L. and E.R. wrote the paper.

Competing interest statement: D.M.M. is the inventor of patents related to the CETSA method and is a cofounder, board member, and employee of Pelago Bioscience AB.

This article is a PNAS Direct Submission.

[1]Present address: School of Basic Medicine, Hubei University of Medicine, Shiyan 442000, Hubei, China.

[2]Present address: Research Center for Plant Functional Genes and Plant Tissue Culture Technology, College of Bioscience and Bioenginering, Jiangxi Agricultural University, Nanchang 330045, Jiangxi, China.

[3]To whom correspondence may be addressed. Email: eurus@psb.vib-ugent.be.

This article contains supporting information online at http://www.pnas.org/lookup/suppl/doi:10.1073/pnas.2118220119/-/DCSupplemental.

Published March 7, 2022.

and BES1/BZR2 transcription factors (14), BIN2/*At*SK21 interacts and phosphorylates the AUXIN RESPONSE FACTOR2 (ARF2) (21). This phosphorylation results in a loss in the DNA binding and repressor activity of ARF2 and facilitates auxin responses (21). BIN2/*At*SK21 also phosphorylates and activates ARF7 and ARF19 to promote lateral root development through an increase in auxin response (22). Moreover, BRs have been shown to control posttranscriptionally the endocytic sorting of PIN-FORMED 2 (PIN2) (23) and stimulate the nuclear abundance and signaling of auxin via repressing the accumulation of PIN-LIKES (PILS) proteins at the endoplasmic reticulum (24).

Here, by adapting the CETSA MS to *Arabidopsis* intact cells and combining it with phosphoproteomics, we discovered that the auxin efflux carrier PIN1 is a substrate of the *At*SKs. We found that phosphorylation mediated by the *At*SKs is required for PIN1 polarity and for leaf venation. In summary, we demonstrate that CETSA MS is a powerful method for the identification of small molecule targets as well as for the discovery of new protein–protein interactions in plant cells.

Results

CETSA Monitoring of Small Molecule–Protein Interactions in Intact *Arabidopsis* Cells. Previously, we had used the Western blot–based CETSA for small molecule target validation in cell lysates of *Arabidopsis* seedlings (6). To extend the use of CETSA to intact plant cells, we adapted the available protocol (10) to *Arabidopsis* cell suspension cultures (*SI Appendix*, Fig. S1). First, we tested whether the plant cell wall complicated the protein isolation by evaluating the efficiency of the freeze–thaw lysis method applied to mammalian cells (10). After washing and resuspension in protein extraction buffer, 100-µL aliquots of cells were freeze–thawed multiple times and the protein concentration of the supernatant was measured with the Bradford protein assay. The protein concentration in the lysate plateaued at the seventh freeze–thaw cycle (*SI Appendix*, Fig. S2*A*). Moreover, considering that plants grow over a wide temperature range, we assessed whether in intact *Arabidopsis* cells, proteins follow a melting profile similar to that in lysates when heated (5, 26). To this end, we heated 100-µL aliquots of *Arabidopsis* cells in protein extraction buffer, heated to different temperatures (from 25 °C to 80 °C) for 2 min, and analyzed the lysates by sodium dodecyl-sulfate polyacrylamide gel electrophoresis (SDS-PAGE) after seven freeze–thaw cycles and centrifugation. As expected, the *Arabidopsis* proteins unfolded and precipitated at high temperature (*SI Appendix*, Fig. S2 *B* and *C*).

Subsequently, as a proof of concept, we aimed to apply CETSA to cells treated with bikinin, an inhibitor of several *At*SKs in *Arabidopsis* (12). Application of bikinin at concentrations of 30 to 50 µM to *Arabidopsis* seedlings induces BR responses that can be measured by changes in the phosphorylation status of the transcription factor BES1/BZR2 (14). To check whether bikinin is effective in *Arabidopsis* cell suspension cultures, we treated cells with 50 µM bikinin for 30 min. As expected, bikinin induced the dephosphorylation of BES1 in the cell cultures similarly to the most active BR, brassinolide (BL) (*SI Appendix*, Fig. S2*D*). Taken together, bikinin can induce BR responses in *Arabidopsis* cell suspension cultures.

Next, we investigated the effect of bikinin on the thermal stability of its direct targets, the ten *At*SKs (12), by means of the adjusted CETSA protocol (*SI Appendix*, Fig. S1) and by using Western blots for detection. In brief, after 30 min of treatment with bikinin or dimethyl sulfoxide (DMSO), the *Arabidopsis* cells were washed, resuspended in protein extraction buffer containing either bikinin or DMSO, and aliquoted into PCR tubes. Then, the aliquots were heated to 12 distinct temperatures (30, 35, 40, 43, 46, 49, 52, 55, 58, 61, 65, and 70 °C) for 2 min. Afterward, the heated cells were lysed through seven freeze–thaw cycles followed by Western blot–based protein detection. As specific antibodies for all *At*SKs are not available, *Arabidopsis* cell suspension cultures overexpressing the hemagglutinin (HA)-tagged *At*SKs were utilized to generate protein-melting curves and to assess the bikinin-induced T_m shifts. First, we examined whether bikinin induced T_m shifts for *At*SK12 and *At*SK13 at a 50-µM concentration, but, surprisingly, found that it stabilized *At*SK13 with a T_m shift of 5.94 °C (*SI Appendix*, Fig. S3*A*), but not *At*SK12 (*SI Appendix*, Fig. S3*B*). By contrast, the thermal stability of the ATP synthase ß (ATPβ), used as a control, was not affected by bikinin. We next performed an isothermal dose–response fingerprinting ($ITDRF_{CETSA}$) for *At*SK12 at 45 °C, a temperature selected between the T_m of *At*SK12 and T_m of *At*SK13 under control (DMSO) conditions and determined the bikinin half-maximum effective concentration (EC_{50}) to be around 70 µM (*SI Appendix*, Fig. S3*C*). To ensure saturation and achieve sufficiently sized T_m shifts for all *At*SKs, we used 250 µM bikinin (Fig. 1). Staining of the cells with the cell viability tracer, fluorescein diacetate (FDA), excluded the potential cytotoxic effect of bikinin when used at high concentrations (*SI Appendix*, Fig. S2*E*). Of the 10 putative bikinin targets (12), *At*SK11, *At*SK12, *At*SK13, BIN2/*At*SK21, *At*SK22, and *At*SK41 showed T_m shifts, whereas the thermal stability of *At*SK23, *At*SK31, *At*SK32, and *At*SK42 was not affected by the small molecule at 250 µM (Fig. 1) as well as the thermal denaturation of the ATPβ control (*SI Appendix*, Fig. S4). Collectively, these results showed that bikinin stabilized most of its targets, indicating that the CETSA protocol was applicable to intact *Arabidopsis* cells.

CETSA MS of Bikinin in Intact *Arabidopsis* Cells. Several recent studies in mammalian cells reported the use of proteome-wide CETSA MS for obtaining a comprehensive view on small molecule–protein interactions through determination of individual temperature shifts (8–10, 27). Therefore, we extended the CETSA protocol as described above (*SI Appendix*, Fig. S1) to the *Arabidopsis* proteome (*SI Appendix*, Fig. S2*D*) by using 50 µM bikinin, the BR response-inducing concentration in cell cultures. Briefly, following the heating at 25, 30, 35, 40, 45, 50, 55, 60, 70, and 80 °C and freeze–thaw cycles, samples were analyzed with a nanoscale liquid chromatography coupled to tandem mass spectrometry (nano LC-MS/MS), whereafter they were digested with trypsin and labeled with 10-plex tandem mass tag (TMT10).

In total, 6,000 proteins were identified, of which the melting profiles were defined for 4,225 proteins in samples treated with both bikinin and DMSO (Dataset S1*A*). Approximately 96% of the identified proteins had a melting temperature within the range of 35 °C to 60 °C (Fig. 2*A* and Dataset S1*A*), of which only 61 proteins displayed a significant change in thermal stability (27 were stabilized and 34 were destabilized) in the presence of 50 µM bikinin (absolute value of T_m shift ≥ 2 °C, analysis of variance [ANOVA]-based F test $P < 0.01$) (Fig. 2*B* and Dataset S1). However, because none of the *At*SKs were identified by the CETSA MS, we examined the protein expression of *At*SKs in *Arabidopsis* cell suspension cultures. Although qRT-PCR revealed expression of all *At*SKs in the cell cultures (*SI Appendix*, Fig. S5*A*), only *At*SK11, *At*SK21, *At*SK31, and *At*SK41, albeit at a low intensity, were detected with shotgun proteomics (*SI Appendix*, Fig. S5*B* and Dataset S2). Given that all *At*SKs were efficiently extracted using the CETSA protocol when overexpressed (Fig. 1), probably the low number of peptides identifying these proteins in cell cultures obstructed the creation of their melting curves (Dataset S2).

As changes in thermal stability had also been observed for downstream effectors of the direct small molecule target, possibly as a result of altered posttranslational modifications or interactions with other proteins (4, 9), we examined whether any of the 61

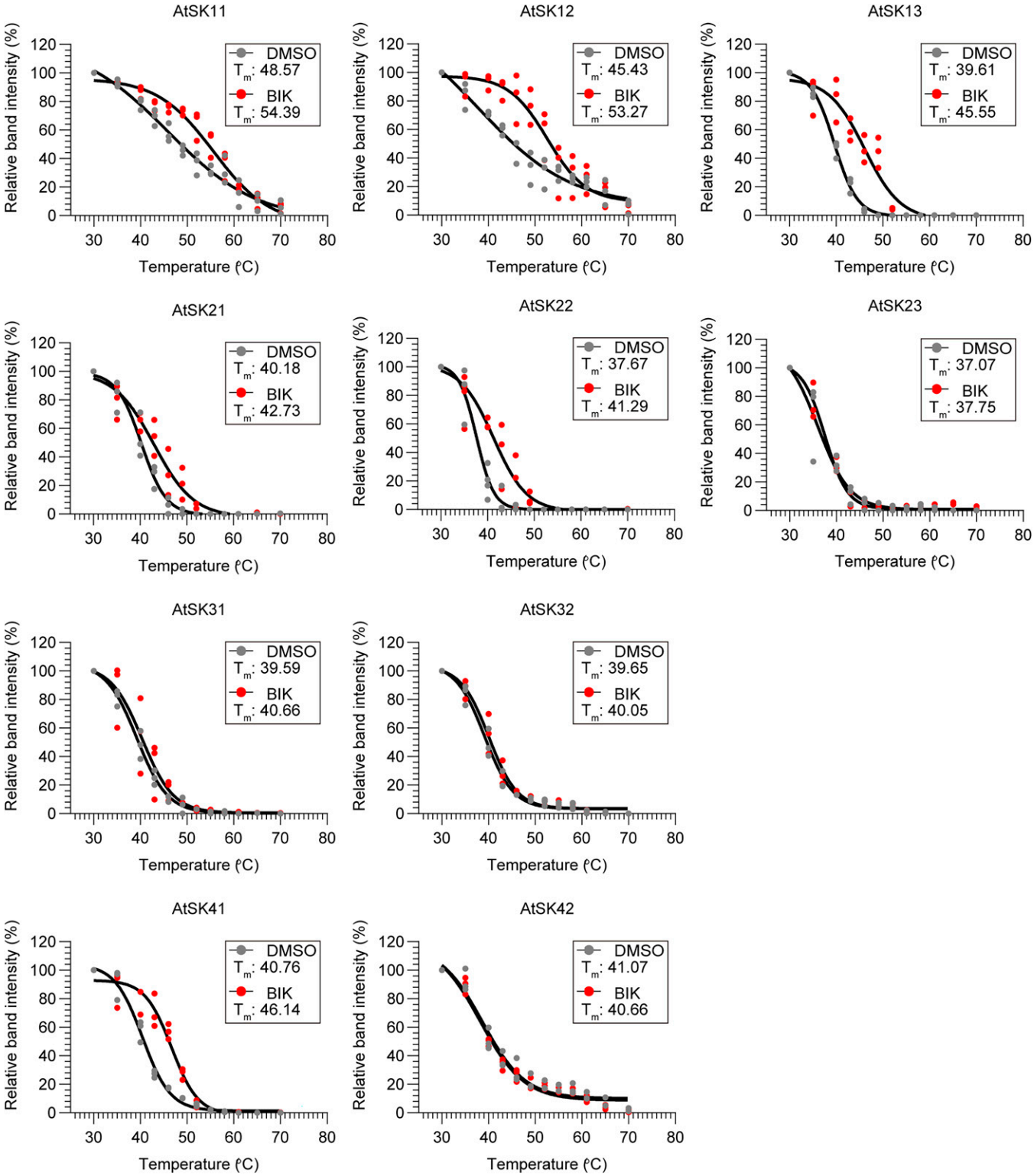

Fig. 1. Bikinin stabilized a subset of the *At*SKs. Thermal denaturation curves for 10 HA-tagged *At*SKs stably overexpressed in *Arabidopsis* cell suspension cultures in the presence of 250 μM bikinin (BIK) or 0.1% (vol/vol) DMSO. The relative band intensities from the Western blot analysis were calculated based on the lowest temperature (30 °C). Melting temperatures (T_m) are indicated. Individual data points are plotted for three biological replicates. For the blots these graphs are based on, see *SI Appendix*, Fig. S13.

proteins ($P < 0.01$) (Dataset S2*B*) functioned together with the *At*SKs and found that only the MITOGEN-ACTIVATED PROTEIN KINASE3 (MPK3), which acts downstream of the known BIN2/*At*SK21 interactor YODA (YDA) (28), exhibited a T_m shift (−2.96 °C, $P < 0.01$). Furthermore, we checked whether any of the 61 proteins with significant T_m shifts were putative *At*SK interactors (*SI Appendix*, Fig. S6) according to the STRING database (29). Based on this analysis, the HOPW1-1-INTERACTING2 (WIN2,

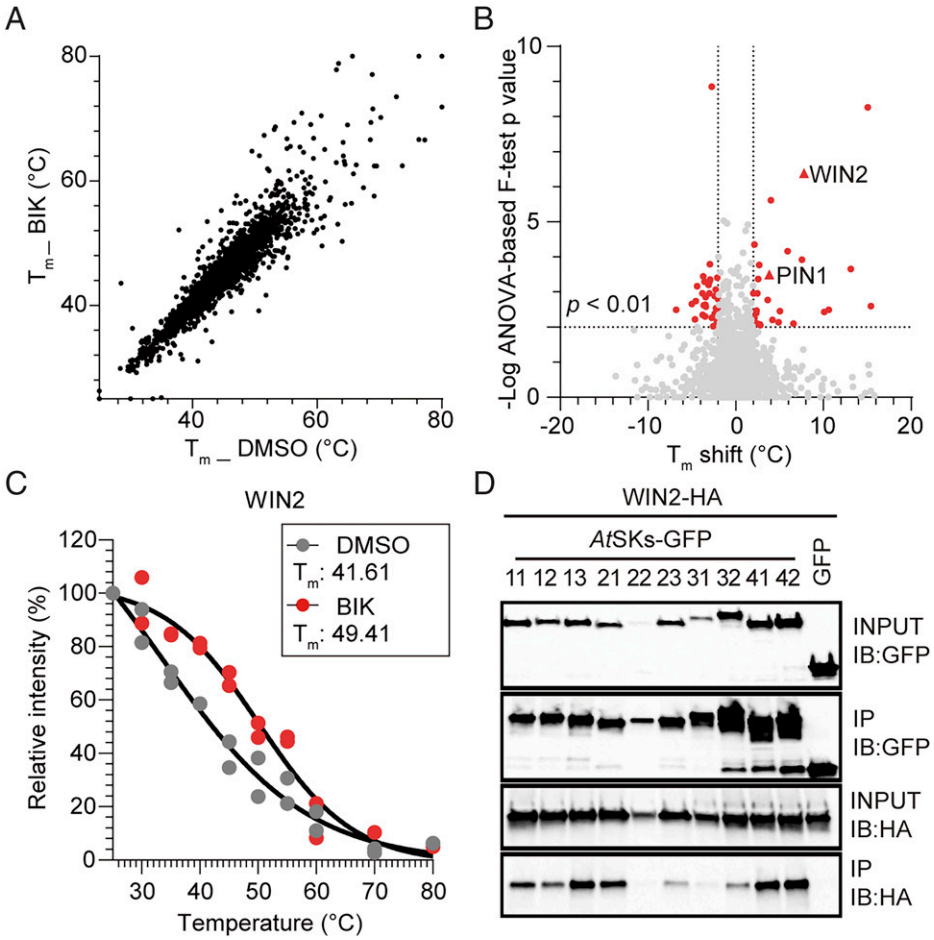

Fig. 2. CETSA MS in the presence of bikinin. (*A*) Melting temperatures of the 4,225 proteins identified in the CETSA MS in the presence of 50 μM BIK or 0.1% (vol/vol) DMSO. (*B*) Distribution of the T_m shifts of all proteins. Proteins in red highlight significant changes (T_m shift > 2 °C, ANOVA-based F test $P < 0.01$). (*C*) Thermal denaturation curves generated for WIN2 in the presence of 50 μM BIK or 0.1% (vol/vol) DMSO subtracted from the CETSA MS in *Arabidopsis* cell suspension cultures. The T_m is indicated. Individual data points are plotted for $n = 2$ technical replicates. (*D*) Coimmunoprecipitation of WIN2 with all *At*SKs when coexpressed in tobacco. The *p35S::WIN2-HA* construct was transiently coexpressed with either *p35S::AtSKs-GFP* or *p35S::GFP* (as a negative control). Proteins were extracted (input) and immunoprecipitated (IP) by means of GFP beads. *At*SKs-GFP, GFP, and WIN2-HA were detected with anti-GFP and anti-HA antibody, respectively. IB, immunoblot.

AT4G31750) (T_m shift = 7.80 °C, $P < 0.01$) (Fig. 2*C*) was selected as a possible *At*SK-interacting protein. Interaction between HA-tagged WIN2 and each of the 10 GFP-tagged *At*SKs was observed by coimmunoprecipitation experiments carried out using tobacco (*Nicotiana tabacum*) cells transiently overexpressing the proteins (Fig. 2*D*). In summary, in cell suspension cultures bikinin affected the thermal stability of the *Arabidopsis* proteome and induced T_m shifts in several proteins that might be putative *At*SK-interacting proteins or *At*SK downstream effectors.

The Phosphoproteome of Bikinin. As, besides MPK3, the proteins with altered thermal stability identified by the CETSA MS (Dataset S1) were neither direct bikinin targets nor known downstream *At*SK effectors, we carried out a phosphoproteomics analysis on bikinin-treated *Arabidopsis* cell suspension cultures. We hypothesized that the putative *At*SK-interacting proteins or *At*SK downstream effectors might modify their phosphorylation state upon inhibition of their kinase activity. *Arabidopsis* cell suspension cultures were treated with 50 μM bikinin or DMSO for 30 min, under the same CETSA MS. The phosphoproteomics analysis revealed that, in total, 9,351 phosphopeptides were mapped to 1,751 proteins (Dataset S3*A*). Bikinin treatment significantly down-regulated ($P < 0.05$) the phosphorylation intensities of 972 phosphosites that belong to 665 proteins (Fig. 3*A* and *SI Appendix*, Fig. S7 and Dataset S3 *B–E*), of which six proteins were known *At*SK-interacting proteins, including, BZR1 (30), ARF2 (21), YDA (28), GLUCOSE-6-PHOSPHATE DEHYDROGENASE6 (G6PD6) (31), TETRATRICOPETIDE-REPEAT THIOREDOXIN-LIKE3 (TTL3) (32), and OCTOPUS (33). In addition, the phosphorylation intensities of 101 phosphosites belonging to 84 proteins were significantly up-regulated ($P < 0.05$) (Fig. 3*A* and *SI Appendix*, Fig. S7 and Dataset S3 *B–E*). Of note, both down-regulated and up-regulated phosphosites were identified in 35 proteins (Fig. 3*A* and Dataset S3 *B–E*). The gene ontology (GO) enrichment analysis (34) revealed that most of the enriched terms for the identified phosphorylation-regulated proteins were related to mRNA splicing, metabolic process, and transport (*SI Appendix*, Fig. S8*A* and Dataset S3*G*). However, of the bikinin-regulated phosphoproteins, only six (phosphorylation down-regulated) proteins showed significant T_m shifts in the CETSA MS (Dataset S3*E*), including the auxin efflux carrier PIN1 (T_m shift = 3.83 °C) (Fig. 3 *A* and *B*). Taken together, only a few proteins identified in the bikinin phosphoproteome displayed bikinin-induced changes in their thermal stability.

***At*SKs Phosphorylate PIN1 and Regulate Its Polarity.** We hypothesized that PIN1 is a direct substrate of the *At*SKs, because the PIN1 protein had been identified in the CETSA MS (Fig. 3 *B*

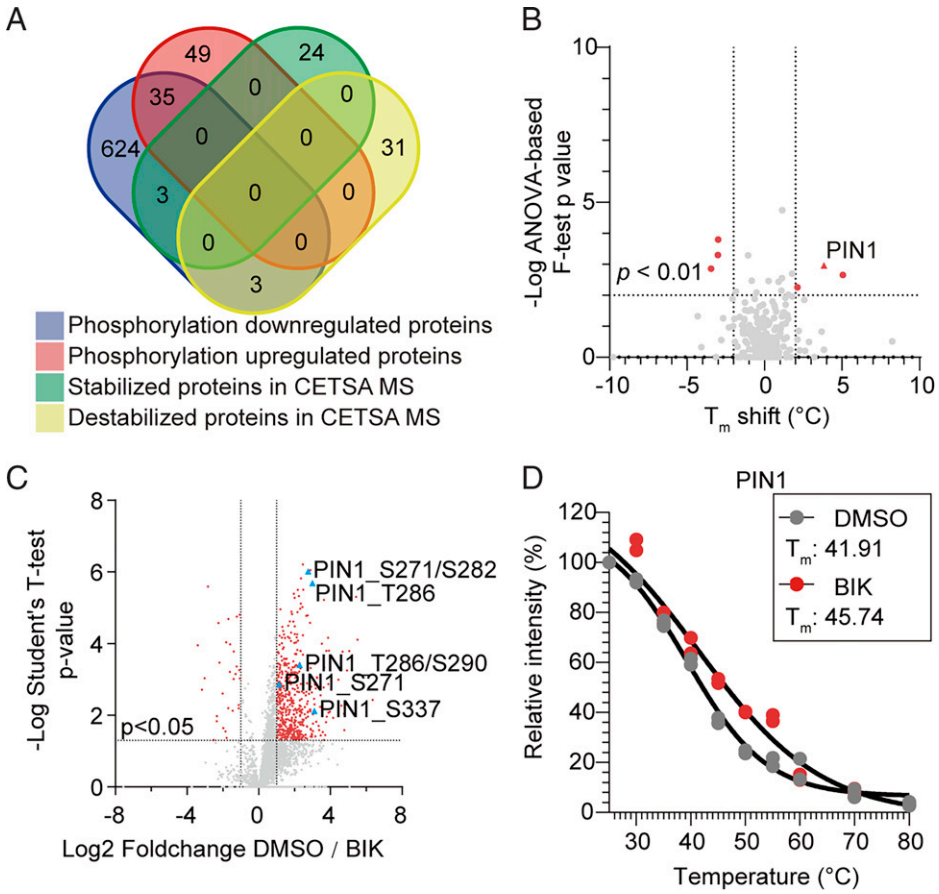

Fig. 3. Identification of PIN1. (*A*) Venn diagram comparing the CETSA MS and the BIK phosphoproteome. Only six proteins (phosphorylation down-regulated) showed significant T_m shifts in CETSA MS. (*B*) T_m shifts distribution of the proteins of which the phosphorylation intensities were down-regulated in the presence of 50 μM BIK. (*C*) Volcano plot representation of the quantitative phosphoproteomics analysis in the presence of 50 μM BIK and 0.1% (vol/vol) DMSO. Diamonds represent phosphopeptides quantified in five biological replicates, each phosphopeptide log2 (fold change) is the average logarithmic ratio of the phosphopeptide abundance in cell suspensions treated with BIK vs. DMSO plotted against the log10 (*P* value) determined by the Student's *t* test. Phosphopeptides of PIN1 are indicated. (*D*) The thermal denaturation curves generated for PIN1 in the presence of 50 μM BIK or 0.1% (vol/vol) DMSO subtracted from the CETSA MS in *Arabidopsis* cell suspension cultures. The T_m is indicated. Individual data points are plotted for $n = 2$ technical replicates.

and *D* and Dataset S1) and the phosphorylation intensities of five residues in the hydrophilic loop (HL) (Ser^{271}, Ser^{282}, Thr^{286}, Ser^{290}, and Ser^{337}) (*SI Appendix*, Fig. S9*A*) were reduced in the presence of 50 μM bikinin (Fig. 3*C* and Dataset S3*C*). To verify this observation, we carried out a protein kinase assay by incubating the polyhistidine (HIS)-tagged HL of PIN1 with HIS-small ubiquitin-like modifier (HIS-SUMO)-tagged *At*SK proteins in an in vitro phosphorylation reaction. The results showed that eight *At*SK proteins phosphorylated the His-PIN1-HL (*SI Appendix*, Fig. S9*B*). Remarkably, four of the five PIN1 residues, of which the phosphorylation was altered by bikinin, had previously been identified as targets of the serine/threonine protein kinases PINOID/AGCVIII kinases (PID/WAGs) (35), D6 Protein Kinases (D6PKs) (36), and MPKs (MPK3, MPK4, and MPK6) (37, 38). Moreover, these residues were conserved (*SI Appendix*, Fig. S9*A*) and essential for the polar localization of the PIN proteins with long HLs (39).

Given the prominent role of phosphorylation in regulating polarity, we next assessed whether treatments with bikinin and BL affected the polar localization of PIN1 and PIN2 in the root meristem by means of immunolocalization. Wild-type *Arabidopsis* plants were treated in liquid medium with 50 μM bikinin, 10 nM BL, and 0.1% (vol/vol) DMSO for 12 h. As anticipated, PIN1 displayed a more apolar localization in the presence of bikinin and BL (Fig. 4 *A* and *B*) than with DMSO, whereas the PIN2 polarity remained unaffected (*SI Appendix*, Fig. S10). To provide genetic evidence for the *At*SK function in PIN1 polarity regulation, we analyzed the PIN1 localization in the root tips of the *At*SK quadruple (*atsk13RNAi bin2 bil1 bil2*, designated $atsk^{quad}$) and sextuple (*atsk11RNAi atsk12RNAi atsk13RNAi bin2-3 bil1 bil2*, designated $atsk^{sext}$) mutants (40). PIN1 had a more apolar localization in the root tips of the $atsk^{quad}$ mutant than the wild-type (Fig. 4 *C* and *D*). Because of the seedling lethality of the $atsk^{sext}$ mutant (40), the plant phenotypes were analyzed in the T1 generation. The $atsk^{sext}$ mutant also displayed an aberrant PIN1 polar localization (Fig. 4 *C* and *D*). Given that PIN1-mediated polar auxin transport regulates the foliar vascular patterning (41), we examined whether *At*SKs were involved in the regulation of leaf venation. Five-day-old wild-type plants were treated in liquid medium with 50 μM bikinin, 10 nM BL, and 0.1% (vol/vol) DMSO for 2 d. As expected, plants treated with bikinin and BL had an abnormal leaf vascular patterning, when compared to the mock control (*SI Appendix*, Fig. S11). Consistent with BR and bikinin treatments, the $atsk^{quad}$ and $atsk^{sext}$ mutants exhibited an aberrant vascular patterning, with missing loops and disconnected upper loops (Fig. 4 *E* and *F*). Subsequently, we examined the PIN1 localization in the leaf veins of $atsk^{quad}$ and $atsk^{sext}$ mutants. As anticipated, $atsk^{quad}$ and $atsk^{sext}$ mutants displayed impaired PIN1 localizations, including missing PIN1 in

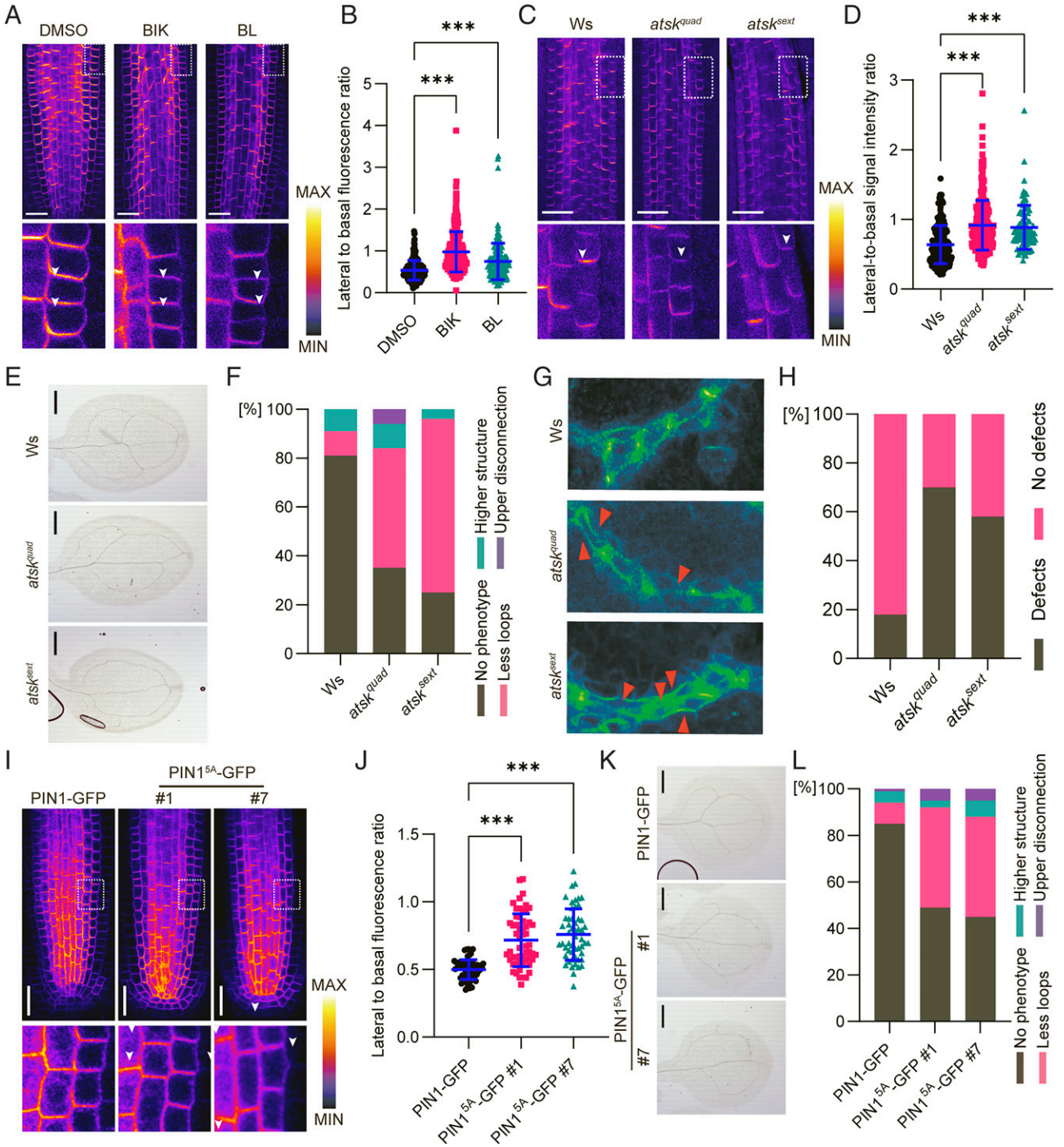

Fig. 4. PIN1 polarity modulation by the *At*SKs. (*A*) Immunolocalization of PIN1 in root tips after 12 h of 50 μM BIK, 10 nM BL, or 0.1% (vol/vol) DMSO treatments. Zoom-ins of areas marked with dashed boxes are shown below each main image. (Scale bars, 20 μm.) (*B*) Quantitative evaluation of *A* showing mean of PIN1 lateral-to-basal signal intensity ratio in endodermal cells. $n > 180$ cells corresponds to a minimum of 15 roots per treatment from three independent experiments. (*C*) Immunolocalization of PIN1 in root tips of Wassilewskija (Ws), *At*SK quadruple (*atsk*^{qudr}), and sextuple (*atsk*^{sext}) mutants. Zoom-ins of areas marked with dashed boxes are shown below each main image. (Scale bars, 20 μm.) (*D*) Quantification of *C* showing mean of PIN1 lateral-to-basal signal intensity ratio in endodermal cells. $n > 95$ cells corresponds to a minimum of 15 roots per treatment from two independent experiments. (*E*) Representative images of venation patterning defects in cotyledons of Ws, *atsk*^{qudr}, and *atsk*^{sext} mutants. (Scale bars, 1 mm.) (*F*) Quantification of venation defects in *atsk*^{qudr} and *atsk*^{sext} mutants ($n > 60$ of each genotype from three independent experiments). (*G*) Immunolocalization of PIN1 in the leaf veins of Ws, *atsk*^{qudr}, and *atsk*^{sext} mutants. Red arrows indicate the defects in PIN1 localization, including missing PIN1, and more PIN1 localizations parallel to the vein axis. (*H*) Quantitative evaluation of *G* showing defects in PIN1 localization; $n > 45$ leaves from five independent experiments. (*I*) Subcellular localization of PIN1-GFP and PIN1-GFP^{5A} in root tip cells. Zoom-ins of areas marked with dashed boxes are shown below each main image. Arrowheads indicate the lateral membrane signal in the endodermal cells. (*J*) Quantitative evaluation of *I* showing mean of PIN1-GFP and PIN1-GFP^{5A} lateral-to-basal signal intensity ratio in endodermal cells. $n > 60$ cells corresponds to a minimum of 15 roots per genotype from three independent experiments. (*K*) Representative images of venation patterning defects in cotyledons of *PIN1pro::PIN1-GFP* and two transgenic lines of *PIN1pro::PIN1*^{5A}*-GFP*. (Scale bars, 1 mm.) (*L*) Quantification of venation defects in *PIN1pro::PIN1-GFP* and two *PIN1pro::PIN1*^{5A}*-GFP* transgenic lines ($n > 60$ of each genotype from three independent experiments). (*B*, *D*, and *J*) Scatter dot plots showing all the individual points with means and SEs. One-way ANOVA with Tukey's post hoc test compared to DMSO or PIN2-GFP, respectively. $^{***}P < 0001$.

some cells and more PIN1 localizations parallel to the vein axis, when compared to the wild-type control (Fig. 4 *G* and *H*).

To test whether the identified five phosphorylation sites were relevant for the *At*SK-mediated regulation of PIN1, we generated phospho-inactive His-PIN1-HL^{5A} by substituting the Thr and Ser residues with Ala. The phosphorylation of His-PIN1-HL^{5A} by BIN2/*At*SK in vitro was reduced but not abolished (*SI Appendix*, Fig. S12*A*), suggesting that more sites were phosphorylated by BIN2/*At*SK21. Next, we introduced the phospho-inactive PIN1^{5A}-GFP (*PIN1pro::PIN1^{5A}-GFP*) into wild-type *Arabidopsis* plants. Noteworthy, 6 of the 26 GFP-positive transgenic plants had naked inflorescence stems in the first generation (*SI Appendix*, Fig. S12*B*), reminiscent of the *pin1* null mutant (42). Then, we examined the localization of PIN1^{5A}-GFP in the root tip cells of wild type–resembling transgenic plants. When expressed at the same levels as the native PIN1-GFP (*pPIN1::PIN1-GFP*) (43) (*SI Appendix*, Fig. S12*C*), PIN1^{5A}-GFP exhibited a more apolar localization in two independent transgenic lines (Fig. 4 *I* and *J*) that, in a similar way to the *atsk^{quad}* and *atsk^{sext}* mutants, had an abnormal vascular patterning in the cotyledons (Fig. 4 *K* and *L*). In summary, these observations show that *At*SK-mediated phosphorylation of PIN1 is important for polar localization and leaf venation.

Discussion

Given the challenges in small molecule target identification in plants (44), experimental strategies, especially label-free methods, are required to facilitate chemical genetics studies. CETSA is such a method that has been proven useful for the detection of direct drug targets and downstream effects of drug-induced perturbations in several cellular systems and tissues (9, 27, 45, 46). In plants, CETSA has been successfully applied for small molecule target validation in cell lysates of *Arabidopsis* (6) and, recently, the thermal profiles of more than 2,000 proteins in *Arabidopsis* lysates have been reported (5, 26). Here, we explored the potential of CETSA to identify the protein targets of the *At*SK kinase inhibitor bikinin (12) in intact *Arabidopsis* cells. In Western blot–based CETSA, bikinin stabilized six of the 10 *At*SKs. As expected, bikinin had no effect on either *At*SK31 or *At*SK42, of which the kinase activity was not inhibited in vitro (12), but surprisingly, on *At*SK23 and *At*SK32 as well, of which the in vitro inhibition of the kinase activity had previously been reported (12). One reason might be that the binding affinity of bikinin to *At*SK23 and *At*SK32 is lower than that to other *At*SKs, thus requiring higher bikinin concentrations to induce the noticeable T_m shifts. Moreover, in a previous study, ∼30% of the target proteins of the promiscuous kinase inhibitor staurosporine did not show T_m shifts (9), suggesting that some protein kinases are not responsive in CETSA.

By combining CETSA with MS, we identified the thermal profiles of 4,225 proteins in the presence of bikinin in *Arabidopsis* cell suspension cultures, of which 61 (1.44%) showed significant T_m shifts (absolute value ≥ 2 °C, ANOVA-based F test $P < 0.01$). Although the CETSA MS assay did not detect any *At*SKs, probably due to their low protein abundance in the cell cultures, MPK3, the substrate of the know BIN2/*At*SK21 interactor YDA (28), was detected. In addition, the thus far unknown interaction between WIN2 (AT4G31750) and *At*SKs was validated in vivo. WIN2 is implicated in the modulation of the defense responses induced by the *Pseudomonas syringae* effector protein HopW1-1 (47). *At*SK11 has been shown to regulate the pattern-triggered immunity and the susceptibility to *P. syringae*, probably through G6PD6 phosphorylation (48). Our data suggest that *At*SK11, as well as its homologs, might regulate the immune responses to *P. syringae* via direct interaction with WIN2.

To demonstrate the capability of CESTA MS to identify proteins that might bind the *At*SKs directly or function in downstream pathways, we carried out a phosphoproteomics analysis in the presence of bikinin. Phosphorylation sites in 665 proteins were down-regulated upon bikinin treatment, comprising six known substrates of the *At*SKs, hence confirming the quality of our data. Noteworthy, the phosphorylation intensities of 84 proteins were up-regulated upon bikinin treatment, indicating that these proteins might be indirect *At*SK targets. The GO enrichment analysis for the bikinin-regulated phosphoproteins revealed that *At*SKs might be involved in the regulation of RNA splicing and protein intracellular transport, like their mammalian homologs (49, 50). Moreover, of all proteins with differential phosphorylation, 76 proteins were also identified by proximity labeling with BIN2/*At*SK21 as a bait (51) (Dataset S3*F*). Thus, we speculate that some of these proteins might be substrates of the *At*SKs. By comparing the CETSA MS and phosphoproteome datasets, we found that the thermal stability of most of these proteins was not affected, even though their phosphorylation intensities were altered by the bikinin treatment. A possible reason might be that either the phosphorylation cannot affect the protein melting behavior or that the bikinin-induced changes in the phosphorylation intensity are not sufficient to induce an important T_m shift for most of these proteins. However, for a few proteins, bikinin had an impact on both the phosphorylation and melting behaviors, indicating that the phosphorylation status might affect the thermal stability of some proteins. Although some studies in human cells reported that phosphorylation affected the protein thermal stability (52), others demonstrated that for most of the proteins, the melting behavior of phosphorylated and nonphosphorylated forms was concordant (53, 54).

Particularly, bikinin reduced the phosphorylation and induced the thermal stabilization of the auxin efflux carrier PIN1. The identified *At*SK phosphorylation sites in the HL of PIN1 are conserved among the PIN proteins (*SI Appendix*, Fig. S9*A*), some of which are essential for their polar localization and the intercellular auxin transport (39). However, although some kinases shared phosphorylation sites in the PIN proteins, for instance PID/WAGs and D6PKs, their corresponding mutants or transgenic overexpression lines affected the PIN polarities differently (35, 36). Moreover, the auxin-regulated receptor CANALIZATION-RELATED AUXIN-REGULATED MALECTIN-TYPE RECEPTOR-LIKE KINASE (CAMEL) (55) and CALCIUM-DEPENDENT PROTEIN KINASE 29 (CPK29) (56) phosphorylate PIN1 and control its polarity via phosphorylation sites that are not shared with other kinases, including PID/WAGs, D6PKs, MPKs, and the *At*SKs (*SI Appendix*, Fig. S9) (55, 56). Therefore, multiple parallel mechanisms for the maintenance of the PIN polarities and activities exist. Our data imply that BRs control the PIN1 phosphorylation and polarity via *At*SKs. Two of the five phosphorylation sites identified in our phosphoproteomics study are also targeted by PID/WAGs and D6PKs, whereas another two phosphorylation sites are targeted by MPK3, MPK4, and MPK6, implying a functional redundancy of *At*SKs with other kinases in the PIN phosphorylation. In addition, bikinin and BR treatments, which inhibit the activity of *At*SKs directly and indirectly, respectively, impaired the PIN1 polarity, indicating that *At*SKs control the polarity of PINs in combination with other kinases. Considering this overlap in the PIN1 phosphorylation sites, understanding of the precise environmental or developmental conditions and upstream pathways that coordinate these kinases will be needed to cooperatively control the PIN polarities. Furthermore, because the PIN phosphorylation induced by D6PKs and PID/WAGs control their activity (57), it will be necessary to examine whether bikinin and exogenous BRs disrupt the auxin transport activity of PIN1 and other PINs. Previous

studies have shown that BRs affect PIN proteins through different mechanisms (23, 58), including transcriptional activation of PIN4 and PIN7 (58). Additionally, BRs and bikinin stabilized PIN2, but not PIN1, to interfere with the auxin distribution in gravistimulated roots (23), whereas BRs partially altered PIN2 polarity via the actin cytoskeleton (59). However, the actin cytoskeleton had been demonstrated not to be required for the polar localization of PIN2 (60). Interestingly, BRs did not affect the PIN2 polarity in our study, although four of the five identified phosphorylation sites are conserved in the HL of PIN2. Together, these data indicate that the mechanisms controlling the polarity and the stability of PINs by BRs differ.

PIN1 has been shown to be expressed in early leaf veins and margins and PIN1-mediated polar auxin transport to be important for the leaf venation pattern in *Arabidopsis* (40). Moreover, MPK6 could regulate the leaf venation pattern probably by regulating the PIN1 phosphorylation and polarity, although the main MPK6-targeted phosphorylation site Ser^{337}, also targeted by *At*SKs, was not involved (37). In addition, the auxin-regulated receptor CAMEL controls the cotyledon venation through modulation of the PIN1 phosphorylation and polarization (55). Our data showed that chemical activity inhibition or genetic knockout of the *At*SKs resulted in impaired PIN1 polarity and defective cotyledon venation patterns, suggesting that BRs control leaf venation via *At*SK-mediated phosphorylation of PIN1.

In summary, we adapted the CETSA MS method for intact *Arabidopsis* cells and demonstrated its ability to identify direct targets and downstream components of the small molecule target proteins. Such information is useful to understand the mode of action of the small molecules and the function of their target proteins. Moreover, we identified PIN1 as a substrate of *At*SKs, uncovering an unknown BR mechanism and auxin cross-talk.

Materials and Methods

Plant Materials and Growth Condition. *A. thaliana* (L.) Heynh. (accession Columbia-0 [Col-0]) was used, except for the *atsk13RNAi bin2-3 bil1 bil2* quadruple and *atsk11RNAi atsk12RNAi atsk13 bil2-3 bil1 bil2* sextuple mutants that were generated in Wassilewskija (Ws) background as previously described (40). The transgenic *Arabidopsis* plant expressing *PIN1pro::PIN1-GFP* had been described previously (43). The growth conditions are described in detail in *SI Appendix, Materials and Methods*.

The experimental procedures for CETSA, CETSA MS, phosphoproteomics, confocal microscopy, in vitro kinase assay, whole-mount in situ immunolocalization of PIN1, immunoprecipitation, qRT-PCR, FDA measurement, and statistical analysis are described in detail in *SI Appendix, Materials and Methods*. The data of CETSA MS and phosphoproteomics analysis are provided in Datasets S1–S3. The primers used in this study are listed in *SI Appendix*, Table S1.

Data Availability. The CETSA MS data have been unloaded to MassIVE (ID: MSV000088545). The phosphoproteomics data have been uploaded to ProteomeXchange (ID: PXD029936). The shotgun proteomics data have been uploaded to ProteomeXchange (ID: PXD030309). All other study data are included in the article and/or supporting information.

ACKNOWLEDGMENTS. We thank Yanhai Yin for providing the anti-BES1 antibody, Johan Winne and Brenda Callebaut for synthesizing bikinin, Yuki Kondo and Hiroo Fukuda for published materials, Tomasz Nodzyński for useful advice, and Martine De Cock for help in preparing the manuscript. This work was supported by the China Scholarship Council for predoctoral (Q.L. and X.X.) and postdoctoral (Y.Z.) fellowships; the Agency for Innovation by Science and Technology for a predoctoral fellowship (W.D.); the Research Foundation-Flanders, Projects G009018N and G002121N (E.R.); and the VIB Tech Watch Fund (E.R.).

1. G. R. Hicks, N. V. Raikhel, Small molecules present large opportunities in plant biology. *Annu. Rev. Plant Biol.* **63**, 261–282 (2012).
2. G. R. Hicks, N. V. Raikhel, Plant chemical biology: Are we meeting the promise? *Front Plant Sci* **5**, 455 (2014).
3. V. Halder, E. Russinova, Understanding the language of drugged plants. *Nat. Chem. Biol.* **15**, 1025–1028 (2019).
4. D. Martinez Molina, P. Nordlund, The cellular thermal shift assay: A novel biophysical assay for in situ drug target engagement and mechanistic biomarker studies. *Annu. Rev. Pharmacol. Toxicol.* **56**, 141–161 (2016).
5. J. D. Volkening, K. E. Stecker, M. R. Sussman, Proteome-wide analysis of protein thermal stability in the model higher plant *Arabidopsis thaliana*. *Mol. Cell. Proteomics* **18**, 308–319 (2019).
6. W. Dejonghe *et al.*, Disruption of endocytosis through chemical inhibition of clathrin heavy chain function. *Nat. Chem. Biol.* **15**, 641–649 (2019).
7. D. Martinez Molina *et al.*, Monitoring drug target engagement in cells and tissues using the cellular thermal shift assay. *Science* **341**, 84–87 (2013).
8. R. Jafari *et al.*, The cellular thermal shift assay for evaluating drug target interactions in cells. *Nat. Protoc.* **9**, 2100–2122 (2014).
9. M. M. Savitski *et al.*, Tracking cancer drugs in living cells by thermal profiling of the proteome. *Science* **346**, 1255784 (2014).
10. H. Franken *et al.*, Thermal proteome profiling for unbiased identification of direct and indirect drug targets using multiplexed quantitative mass spectrometry. *Nat. Protoc.* **10**, 1567–1593 (2015).
11. K. V. M. Huber *et al.*, Proteome-wide drug and metabolite interaction mapping by thermal-stability profiling. *Nat. Methods* **12**, 1055–1057 (2015).
12. B. De Rybel *et al.*, Chemical inhibition of a subset of *Arabidopsis thaliana* GSK3-like kinases activates brassinosteroid signaling. *Chem. Biol.* **16**, 594–604 (2009).
13. Z.-Y. Wang *et al.*, Nuclear-localized BZR1 mediates brassinosteroid-induced growth and feedback suppression of brassinosteroid biosynthesis. *Dev. Cell* **2**, 505–513 (2002).
14. Y. Yin *et al.*, BES1 accumulates in the nucleus in response to brassinosteroids to regulate gene expression and promote stem elongation. *Cell* **109**, 181–191 (2002).
15. C. Li, B. Zhang, H. Yu, GSK3s: Nodes of multilayer regulation of plant development and stress responses. *Trends Plant Sci.* **26**, 1286–1300 (2021).
16. T.-W. Kim *et al.*, Brassinosteroid signal transduction from cell-surface receptor kinases to nuclear transcription factors. *Nat. Cell Biol.* **11**, 1254–1260 (2009).
17. Z. Yan, J. Zhao, P. Peng, R. K. Chihara, J. Li, BIN2 functions redundantly with other Arabidopsis GSK3-like kinases to regulate brassinosteroid signaling. *Plant Physiol.* **150**, 710–721 (2009).
18. W. Rozhon, J. Mayerhofer, E. Petutschnig, S. Fujioka, C. Jonak, ASKθ, a group-III Arabidopsis GSK3, functions in the brassinosteroid signalling pathway. *Plant J.* **62**, 215–223 (2010).
19. P. Patel, J. R. Woodgett, "Glycogen synthase kinase 3: A kinase for all pathways?" in Current Topics in Developmental Biology, vol. 123 Protein Kinases in Development and Disease, A. Jenny, Ed. (Academic Press, 2017), pp. 277–302.
20. A. Nakamura *et al.*, Brassinolide induces *IAA5*, *IAA19*, and DR5, a synthetic auxin response element in Arabidopsis, implying a cross talk point of brassinosteroid and auxin signaling. *Plant Physiol.* **133**, 1843–1853 (2003).
21. G. Vert, C. L. Walcher, J. Chory, J. L. Nemhauser, Integration of auxin and brassinosteroid pathways by Auxin Response Factor 2. *Proc. Natl. Acad. Sci. U.S.A.* **105**, 9829–9834 (2008).
22. H. Cho *et al.*, A secreted peptide acts on BIN2-mediated phosphorylation of ARFs to potentiate auxin response during lateral root development. *Nat. Cell Biol.* **16**, 66–76 (2014).
23. K. Retzer *et al.*, Brassinosteroid signaling delimits root gravitropism via sorting of the *Arabidopsis* PIN2 auxin transporter. *Nat. Commun.* **10**, 5516(2019).
24. L. Sun *et al.*, PIN-LIKES Coordinate brassinosteroid signaling with nuclear auxin input in *Arabidopsis thaliana*. *Curr. Biol.* **30**, 1579–1588 (2020).
25. M. Ackerman-Lavert *et al.*, Auxin requirements for a meristematic state in roots depend on a dual brassinosteroid function. *Curr. Biol.* **31**, 4462–4472 (2021).
26. A. Jarzab *et al.*, Meltome atlas-thermal proteome stability across the tree of life. *Nat. Methods* **17**, 495–503 (2020).
27. A. Mateus *et al.*, Thermal proteome profiling in bacteria: Probing protein state *in vivo*. *Mol. Syst. Biol.* **14**, e8242 (2018).
28. T.-W. Kim, M. Michniewicz, D. C. Bergmann, Z.-Y. Wang, Brassinosteroid regulates stomatal development by GSK3-mediated inhibition of a MAPK pathway. *Nature* **482**, 419–422 (2012).
29. D. Szklarczyk *et al.*, STRING v10: Protein-protein interaction networks, integrated over the tree of life. *Nucleic Acids Res.* **43**, D447–D452 (2015).
30. J.-X. He, J. M. Gendron, Y. Yang, J. Li, Z.-Y. Wang, The GSK3-like kinase BIN2 phosphorylates and destabilizes BZR1, a positive regulator of the brassinosteroid signaling pathway in *Arabidopsis*. *Proc. Natl. Acad. Sci. U.S.A.* **99**, 10185–10190 (2002).
31. S. Dal Santo *et al.*, Stress-induced GSK3 regulates the redox stress response by phosphorylating glucose-6-phosphate dehydrogenase in *Arabidopsis*. *Plant Cell* **24**, 3380–3392 (2012).
32. V. Amorim-Silva *et al.*, TTL proteins scaffold brassinosteroid signaling components at the plasma membrane to optimize signal transduction in *Arabidopsis*. *Plant Cell* **31**, 1807–1828 (2019).

33. P. Anne *et al.*, OCTOPUS negatively regulates BIN2 to control phloem differentiation in *Arabidopsis thaliana*. *Curr. Biol.* **25**, 2584–2590 (2015).
34. S. X. Ge, D. Jung, R. Yao, ShinyGO: A graphical gene-set enrichment tool for animals and plants. *Bioinformatics* **36**, 2628–2629 (2020).
35. J. Friml *et al.*, A PINOID-dependent binary switch in apical-basal PIN polar targeting directs auxin efflux. *Science* **306**, 862–865 (2004).
36. I. C. R. Barbosa, M. Zourelidou, B. C. Willige, B. Weller, C. Schwechheimer, D6 PROTEIN KINASE activates auxin transport-dependent growth and PIN-FORMED phosphorylation at the plasma membrane. *Dev. Cell* **29**, 674–685 (2014).
37. W. Jia *et al.*, Mitogen-activated protein kinase cascade MKK7-MPK6 plays important roles in plant development and regulates shoot branching by phosphorylating PIN1 in Arabidopsis. *PLoS Biol.* **14**, e1002550 (2016).
38. M. Dory *et al.*, Coevolving MAPK and PID phosphosites indicate an ancient environmental control of PIN auxin transporters in land plants. *FEBS Lett.* **592**, 89–102 (2018).
39. I. C. R. Barbosa, U. Z. Hammes, C. Schwechheimer, Activation and polarity control of PIN-FORMED auxin transporters by phosphorylation. *Trends Plant Sci.* **23**, 523–538 (2018).
40. Y. Kondo *et al.*, Plant GSK3 proteins regulate xylem cell differentiation downstream of TDIF-TDR signalling. *Nat. Commun.* **5**, 3504 (2014).
41. E. Scarpella, D. Marcos, J. Friml, T. Berleth, Control of leaf vascular patterning by polar auxin transport. *Genes Dev.* **20**, 1015–1027 (2006).
42. T. Vernoux, J. Kronenberger, O. Grandjean, P. Laufs, J. Traas, PIN-FORMED 1 regulates cell fate at the periphery of the shoot apical meristem. *Development* **127**, 5157–5165 (2000).
43. E. Benková *et al.*, Local, efflux-dependent auxin gradients as a common module for plant organ formation. *Cell* **115**, 591–602 (2003).
44. W. Dejonghe, E. Russinova, Plant chemical genetics: From phenotype-based screens to synthetic biology. *Plant Physiol.* **174**, 5–20 (2017).
45. J. M. Dziekan *et al.*, Identifying purine nucleoside phosphorylase as the target of quinine using cellular thermal shift assay. *Sci. Transl. Med.* **11**, eaau3174 (2019).
46. J. Perrin *et al.*, Identifying drug targets in tissues and whole blood with thermal-shift profiling. *Nat. Biotechnol.* **38**, 303–308 (2020).
47. M. W. Lee, J. Jelenska, J. T. Greenberg, Arabidopsis proteins important for modulating defense responses to *Pseudomonas syringa*e that secrete HopW1-1. *Plant J.* **54**, 452–465 (2008).
48. H. Stampfl, M. Fritz, S. Dal Santo, C. Jonak, The GSK3/Shaggy-like kinase ASKα contributes to pattern-triggered immunity. *Plant Physiol.* **171**, 1366–1377 (2016).
49. A. Adachi *et al.*, Golgi-associated GSK3β regulates the sorting process of post-Golgi membrane trafficking. *J. Cell Sci.* **123**, 3215–3225 (2010).
50. M. Y. Shinde *et al.*, Phosphoproteomics reveals that glycogen synthase kinase-3 phosphorylates multiple splicing factors and is associated with alternative splicing. *J. Biol. Chem.* **292**, 18240–18255 (2017).
51. T.-W. Kim *et al.*, Application of TurboID-mediated proximity labeling for mapping a GSK3 kinase signaling network in Arabidopsis. *bioRxiv*, 636324 (2019).
52. J. X. Huang *et al.*, High throughput discovery of functional protein modifications by Hotspot Thermal Profiling. *Nat. Methods* **16**, 894–901 (2019).
53. C. M. Potel *et al.*, Impact of phosphorylation on thermal stability of proteins. *Nat. Methods* **18**, 757–759 (2021).
54. I. R. Smith *et al.*, Identification of phosphosites that alter protein thermal stability. *Nat. Methods* **18**, 760–762 (2021).
55. J. Hajný *et al.*, Receptor kinase module targets PIN-dependent auxin transport during canalization. *Science* **370**, 550–557 (2020).
56. H. Lee, A. Ganguly, S. Baik, H.-T. Cho, Calcium-dependent protein kinase 29 modulates PIN-FORMED polarity and *Arabidopsis* development via its own phosphorylation code. *The Plant Cell* **33**, 3513–3531 (2021).
57. M. Zourelidou *et al.*, Auxin efflux by PIN-FORMED proteins is activated by two different protein kinases, D6 PROTEIN KINASE and PINOID. *eLife* **3**, e02860 (2014).
58. A. Nakamura, H. Goda, Y. Shimada, S. Yoshida, Brassinosteroid selectively regulates *PIN* gene expression in Arabidopsis. *Biosci. Biotechnol. Biochem.* **68**, 952–954 (2004).
59. M. Lanza *et al.*, Role of actin cytoskeleton in brassinosteroid signaling and in its integration with the auxin response in plants. *Dev. Cell* **22**, 1275–1285 (2012).
60. M. Glanc, M. Fendrych, J. Friml, PIN2 polarity establishment in *Arabidopsis* in the absence of an intact cytoskeleton. *Biomolecules* **9**, 222 (2019).